RSC Advances




ROYAL SOCIETY OF CHEMISTRY

www.rsc.org/advances

# Bubble-assisted growth of hollow palladium nanospheres with structure control allowing very thin shells for highly enhanced catalysis

**Shaochun Tang, Sascha Vongehr, Xiangyu Wang, Yongguang Wang and Xiangkang Meng***

***Received (in XXX, XXX) Xth XXXXXXXXX 200X, Accepted Xth XXXXXXXXX 200X***
***First published on the web Xth XXXXXXXXX 200X***
**DOI: 10.1039/b000000x**

**Palladium shells are prepared via a one-step solvothermal synthesis involving nanobubbles as soft templates although no stabilizer is present, while still allowing control over diameter, thickness, and grain size, leading to grain-monolayer thin and porous shells with very high and durable electrocatalytic activity.**

Hollow nanostructures attract much interest due to their high specific surface area.[1] Metallic, hollow nanospheres become important in catalysis,[2] biomedicine,[3] as optical devices,[4] and so on. Typically, they are prepared by metal deposition onto carbon, silica, or polymer spheres which are removed by thermal treatment[5] or etched away.[6,7] Galvanic replacement of silver and cobalt as sacrificial templates,[8] and co-assembly of metal nanoparticles (NPs) with organic molecules[9] are also used. These require many steps[1-9] or hazardous reagents.[6] To achieve a high catalytic activity, the grain size and shell width should be as small as possible, but the usual techniques damage especially the desired thin shells.[7,11]

Bubble-assisted synthesis is a green method for large-scale fabrication of hollow spheres. However, due to their high Laplace pressure, nanobubbles dissolve too fast.[12] There has been only limited success with bubble assisted preparation of nanoshells,[13-15] and stabilizing surfactants are deemed crucial. Strong adhesion of surfactants in pores makes their complete removal difficult, impacting catalytic performance. Herein we report on Pd shells from a novel one-step solvothermal synthesis using hydrogen nanobubbles as soft templates without surfactants. Shell diameter, thickness, and grain size is controlled by concentrations ($C_{HCOOH}$ and $PdCl_4^{2-}$ concentration $C_{Pd}$), and temperature $T$. The method allows small grain, grain-monolayer thin, incomplete shells superior for catalysis. The growth mechanism and the stability of the bubbles are discussed. We also studied the catalytic performance by benchmarking with formic acid oxidation, comparing between Pd NPs, Pd-black and our Pd-shell products with different shell thicknesses.

Fig. 1a presents the product from a typical synthesis. The isolated spherical particles have rough surfaces and a diameter of $d$ = (145 ± 25) nm based on the survey of 50 randomly chosen spheres (Fig. 1b). The width of the size distribution is relatively large, which conceivably may result from that the equilibrium bubble size changes over time, but such is for now mere speculation. The TEM image (Fig. 1c) shows the spheres' cavities; shell thickness $h$ is only (16 ± 4) nm.

The SAED pattern (inset) recorded from a shell reveals a polycrystalline nature with diffraction rings corresponding to facets of face-center-cubic (fcc) Pd. Magnification (Fig. 1d) and HRTEM from a sphere's edge (Fig. 1e) show the (6 ± 2)

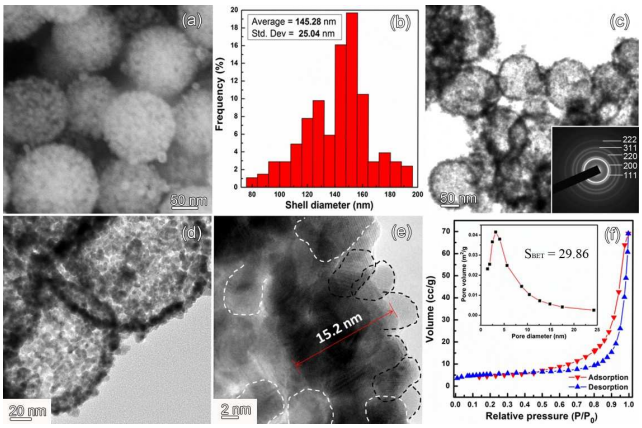


**Fig. 1** SEM (a), histogram of diameters for 50 shells (b), TEM (c-d) with SAED pattern inset in c, and HRTEM image (e). $N_2$ sorption isotherm (f) of the typical product and its pore-size distribution (inset).

nm single-crystalline grains; their crystallographic orientations lie in random directions. The BET area is 30 $m^2/g$ (Fig. 1f), about five times larger than when assuming only the outside surfaces of dense smooth shells contribute. In that case, the specific surface equals the outer surface $A = 4\pi (d/2)^2$ divided by the shell's mass $m = V \times \rho_{Pd}$, with shell volume $V = (4\pi/3)\,[(d/2)^3 - (d/2 - h)^3]$. This estimate gives about 6 $m^2/g$. An about three times larger BET indicates merely a rough surface, but the factor of five indicates that there is already significant porosity (so that the assumption of a dense shell with bulk Pd density $\rho_{Pd}$ is not valid).

With $C_{HCOOH}$ equal or below 0.72 M, only NP aggregates with irregular shapes are obtained (Fig. S1a). Increasing $C_{HCOOH}$ to 1.44 M results in shells with diameters of (85 ± 13) nm, but irregular and large aggregates are still observed (Fig. S1b). At $C_{HCOOH}$ = 2.16 M, the diameter is (122 ± 22) nm (Fig. 2a). A $C_{HCOOH}$ of 2.88 M results in the already discussed sample shown in Fig. 1c. At 3.60 M and 4.32 M, the diameter increases to (175 ± 28) nm and (250 ± 30) nm (Fig. 2b and c). Around 5.04 M, most of the resulting 360 nm diameter shells are broken and the surface is covered incompletely (Fig. 2d). Please notice that the front and back halves of a shell overlap each other in the image. The uncovered areas of the shell are therefore even larger than it appears. Further increasing $C_{HCOOH}$ to 5.76 M results in only debris of broken shells (Fig. S1c). When $C_{HCOOH}$ is above 6.0 M, no hollow spheres but network-like nanostructures are obtained (Fig. S1d).

The thicknesses $h$ of the shells (insets of Fig. 2) obtained with different $C_{HCOOH}$ of 1.44, 2.16, 2.88, 3.60, 4.32 and 5.04 M are 13, 21, 16, 12, 10, and 7 nm, respectively (all with

standard deviations of ~ 4 nm). Since the amount of Pd was kept constant throughout ($C_{Pd}$ was not changed), one expects that $h$ decreases with increasing diameter. The diameter changes almost linearly with $C_{HCOOH}$ (Fig. 2e). However, $d$ increases by roughly a factor of three while $h$ decreases roughly by *the same* factor of three from 21 to 7 nm (we omit the 85 nm diameter shells, which come together with many irregular aggregates, from this analysis). This does not reflect the square law dependence between surface and diameter! The number of shells, which is around $10^{11}$ as calculated from the amount of used Pd, therefore decreases with increasing $C_{HCOOH}$. It should be noted that at a high $C_{HCOOH}$ of 5.04 M, the shells are roughly grain-monolayers because the average thickness is not even twice the average grain size, as indicated by HRTEM images. Even higher concentrations will lead to less surface coverage, which can no longer maintain a stable spherical shape, as confirmed by the debris obtained with $C_{HCOOH}$ = 5.76 M. The BET specific surface area of the 5.04 M product is measured to be 87.5 $m^2/g$. Addition of 0.2 mmol CTAB and other conditions being the same ($C_{HCOOH}$ = 5.04 M) shows that $d$ is widely distributed and the shells are thick (Fig. S2). Further increasing $C_{HCOOH}$ can no longer achieve monolayer Pd shells. This indicates that an addition of surfactants into the reaction system does not facilitate the formation of shells but makes size control difficult.

Keeping $C_{HCOOH}$ at 2.88 M, shells do not form when $C_{Pd}$ is below 1.0 mM (Fig. S3a). The typical $C_{Pd}$ of 1.5 mM results in a thickness of 16 nm. At 2.5 mM, the shell thickness $h$ increases to (23 ± 4) nm (Fig. S4a), and at 4.0 mM, the shells are (28 ± 5) nm thick but irregular NP aggregates start to be observed (Fig. S4b). Beyond 5.0 mM, large 3D networks form (Fig. S3b). The diameter of the shells stays surprisingly constant when changing $C_{Pd}$. Therefore, the dependence between the total amount of Pd and $h$ again proves a varying number of bubbles. This is here due to that the Pd is actively involved in turning HCOOH into $H_2$. Since the grain size stays constant, the number density of Pd NPs increases linearly with $C_{Pd}$. More Pd results in more bubbles, suggesting already that the bubbles grow on the Pd, so the growth mechanism is more complex than just having NPs attach to pre-existing bubbles or micelles as usual[9] with a surfactant facilitated synthesis. The diameter is indeed robustly dependent only on $C_{HCOOH}$, as confirmed by the product from $C_{Pd}$ =4.0 mM and $C_{HCOOH}$ =5.04 M: the diameter is as expected 360 nm again, and $h$ thus lowered to 18 nm (Fig. S4c).

Reaction temperature $T$ influences crystal growth and thus determines the grain size. Fig. S4d-f shows TEM images of Pd shells obtained with different $T$ while keeping other parameters typical ($C_{HCOOH}$ = 2.88 M and $C_{Pd}$ = 1.5 mM). This synthesis series reliably obtains hollow spheres with a diameter of ~145 nm. However, the average grain sizes obtained at 60, 100, 160 and 200 °C are 4 ± 2 nm (Fig. S4d), 6 ± 2 nm (Fig. S4e), 11 ± 4 nm, and 21 ± 7 nm (Fig. S4f). The XRD patterns (Fig. S4g) verify the products' high purity and crystallinity. The four peaks at 39.8°, 46.3°, 67.6° and 81.9° correspond to the (111), (200), (220) and (311) of fcc Pd. The peak broadening is associated with the grain size. According to the Scherrer equation, the average grain sizes from different $T$ of 60, 100, and 200 °C are about 5, 8, and 22 nm, consistent with the TEM results. The average grain size's dependence on $T$ is depicted in Fig. S4h. Table S1 summarizes reaction parameters and corresponding sizes, demonstrating that the average $d$, $h$, and grain size are controllable.

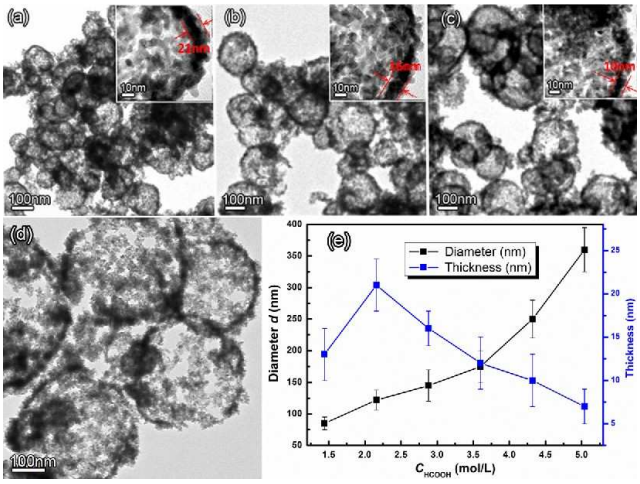


**Fig. 2** TEM images of the Pd products obtained with different $C_{HCOOH}$ of 2.16 (a), 3.60 (b), 4.32 (c), and 5.04 M (d), and the dependence of the diameter and shell thickness on $C_{HCOOH}$ (e).

At an autoclave filling ratio of $r$ = 100%, bubbles cannot form in the incompressible solvent. When $r$ is increased from the typical 60% to 65%, shell diameters are not uniform (Fig. S5a). At 75%, no hollow spheres but networks are obtained (Fig. S5b). If $r$ is decreased to 50%, only debris of shells is obtained (see Fig. S5c-d). Although the variation of $r$ seemed small and the large effects thus surprising, an estimation of the pressures in the reaction system indeed tripled when changing $r$ from 50% to 70%.

The growth mechanism of the Pd shells must be discussed together with the stability of the bubbles. HCOOH reduces Pd(II) into Pd(0) which gives a suspension of Pd NPs whose grain size depends on $T$. Once reduction of $PdCl_4^{2-}$ comes to a finish and many Pd grains are present, they decompose HCOOH into $H_2$ and $CO_2$. The Pd ions are reduced and exhausted by nucleation and production of Pd NPs before the growth into shells happens. Therefore, when considering the bubbles as they participate in the growth, HCOOH still reducing Pd ions is no longer a process that competes for HCOOH, thus it does not need to be considered. $CO_2$ dissolves well in water, but $H_2$ not. Therefore, $H_2$ will become oversaturated. Nevertheless, homogeneous bubble nucleation needs extreme oversaturations, hence bubble nucleation is known to be generally heterogeneous. Heterogeneous nucleation easily starts at the rough Pd grain surfaces where $H_2$ concentration is large. In this surfactant-free system, the bubbles cannot exist independently, waiting for the NPs to assemble on them. Since the NPs favor an interfacial location (that is why they assemble on bubbles at all), the Pd never separates from the bubbles they produce. Bubbles and attached grains fuse into larger bubble/grain systems, so the bubble size initially varies. That $H_2$ is produced at the bubbles is again relevant, because the concentration directly at the bubble determines the diffusive flow equilibrium through the

bubble surface.[16]

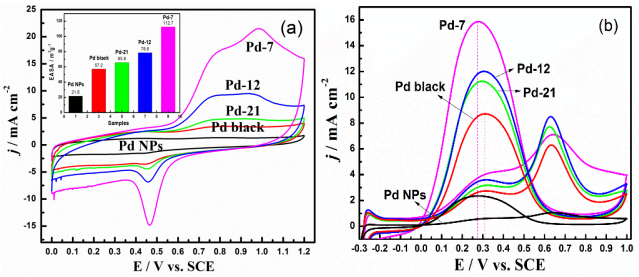


**Fig. 3** Cyclic voltammograms of the different Pd catalysts in 0.5 M $H_2SO_4$ (a) and 0.5 M $H_2SO_4$ + 0.25 M HCOOH (b) at a scan rate of 50 mV/s. The inset of a shows EASA values calculated from the CV curves.

Formic acid oxidation was used to characterize the catalytic activity of the Pd shells in comparison with commercial Pd black (Sigma-Aldrich, 99.8 wt%) and (5 ± 2) nm Pd NPs (Fig. S6a and b). Fig. 3a shows cyclic voltammograms (CVs) of glassy carbon electrodes (GCEs) modified with the different Pd materials [Pd black, Pd NPs, and 21, 12, as well as 7 nm thick Pd shells ("Pd-21", "Pd-12", and "Pd-7")] in $N_2$-saturated 0.5 M $H_2SO_4$ solution at a scan rate of 50 mV/s. The Pd mass loading on the GCEs is the same for all the tests, as ensured by the preparation of the GCE (see Supplementary Information). The peak appearing at 0.47 V (vs. SCE) in the forward scan originates from desorption of atomic hydrogen. The electrochemically active surface area (EASA) of the GCEs was determined by the charge under the hydrogen desorption peak.[17] The specific EASA of the Pd-7 is calculated to be 112.7 $m^2/g$, which is more than five times that of Pd NPs (21.8 $m^2/g$), and significantly higher than that of the commercial Pd black (57.2 $m^2/g$) and those of the other Pd shells (78.6 and 65.8 $m^2/g$ for the Pd-12 and Pd-21).

Fig. 3b shows CVs of the GCEs in a $N_2$-saturated 0.5 M $H_2SO_4$ solution containing 0.25 M HCOOH. In the potential scans in both positive and negative directions, the overall current density for formic acid oxidation measured on Pd-7 is the highest, in agreement with the ECSAs. The peak current density at the positive scan on Pd-7 is 15.95 mA/$cm^2$, almost 8 times that on Pd NPs (2.05 mA/$cm^2$) and almost twice that on commercial Pd black (8.62 mA/$cm^2$). The peak potential of the formic acid oxidation for the Pd-7 electrode is decreased by 0.05 V. These results confirm the expectations from the discussion of the nanostructure. The enhancement of activity can be attributed to the hollow chamber[11] and the richness of the interfaces between small grains[18] providing highly dispersed Pd active sites, which is why smaller grains as well as thinner shells, which present all grains and more of their interfaces accessibly to the solution (high EASA), are preferable. The catalysts have been used repetitively for more than three times without significant loss of activity. The hollow chamber is also well preserved after successive catalytic reactions (Fig. S7a). That the Pd catalyst retains its activity during repetitive uses is also demonstrated by XPS analysis in Fig. S7b. A further increase of the activity can be expected from an optimization of these parameters, namely finding the optimum pair of small grain size and thin shells possible together via the respective synthesis conditions.

In summary, spherical Pd shells were prepared by a one-step solvothermal synthesis, where formic acid reducer provides also nanobubbles serving as soft templates. Control over the diameter (85 to 360 nm), shell thickness (7 to 28 nm), and grain size (4 to 21 nm) are achieved by adjusting $C_{HCOOH}$, $C_{Pd}$, and $T$. The grain-monolayer thin, porous shells with a high specific surface area of 87.5 $m^2/g$ possess a very high activity in electrocatalysis, their hollow chambers are stable when the product is stored long term in ethanol for example. The shells can be used many times, showing a good potential for direct fuel cell applications. The method should be extendable to platinum. The catalytic performance can be further optimized by aiming for smaller grain sizes obtained at lower temperatures. Changing $T$ also shifts the upper limit on $C_{HCOOH}$ responsible for thin shells, therefore, the location of the optimum product in parameter space is not a trivial matter. The open questions concerning the bubble facilitated growth mechanism should inspire more theoretical and experimental work.

This work was jointly supported by the PAPD, the Natural Science Foundation of Jiangsu Province, the National Natural Science Foundation of China and the State Key Program for Basic Research of China.

## Notes and references

*Institute of Materials Engineering, National Laboratory of Solid State Microstructures and College of Engineering and Applied Sciences, Nanjing University, Jiangsu, P. R. China.*
*Tel: (+86) 25 8368 5585. E-mail: mengxk@nju.edu.cn*
*† Electronic Supplementary Information (ESI) available: [Experimental section, TEM images showing Pd products obtained with different $C_{HCOOH}$, different $C_{Pd}$, and varying r]. See DOI: 10.1039/b000000x/*

1 Y. D. Yin, R. M. Rioux, C. K. Erdonmez, S. Hughes, G. A. Somorjai and A. P. Alivisatos, *Science*, 2004, **304**, 711.
2 F. Wang, C. H. Li, L. D. Sun, C. H. Xu, J. F. Wang, J. C. Yu and C. H. Yan, *Angew. Chem. Int. Ed.*, 2012, **51**, 4872.
3 L. R. Hirsch, J. B. Jackson, A. Lee, N. J. Halas and J. West, *Anal. Chem.*, 2003, **75**, 2377.
4 P. R. Selvakannan and M. Sastry, *Chem. Commun.*, 2005, 1684.
5 H. M. Du, L. F. Jiao, Q. H. Wang, J. Q. Yang, L. J. Guo, Y. C. Si, Y. J. Wang and H. T. Yuan, *Nano Res.*, 2013, **6**, 87.
6 S. W. Kim, M. Kim, W. Y. Lee and T. Hyeon, *J. Am. Chem. Soc.*, 2002, **124**, 7642.
7 R. M. Garcia, Y. J. Song, R. M. Dorin, H. R. Wang, P. Li, F. Swol and J. A. Shelnutt, *Chem. Commun.*, 2008, 2535.
8 Y. Sun, B. Bayers and Y. N. Xia, *Adv. Mater.*, 2003, **15**, 641.
9 M. S. Wong, J. N. Cha, K. S. Choi, T. J. Deming and G. D. Stucky, *Nano Lett.*, 2002, **2**, 583.
10 X. L. Fang, Z. H. Liu, M. F. Hsieh, M. Chen, P. X. Liu, C. Chen and N. F. Zheng, *ACS Nano*, 2012, **6**, 4434.
11 H. Li, J. Liu, S. H. Xie, M. H. Qiao, W. L. Dai, Y. F. Lu and H. X. Li, *Adv. Funct. Mater.*, 2008, **18**, 3235.
12 M. Matsumoto and K. Tanaka, *Fluid Dyn. Res.*, 2008, **40**, 546.
13 Z. C. Wu, K. Yu, S. D. Zhang and Y. Xie, *J. Phys. Chem. C*, 2008, **112**, 11307.
14 X. J. Zhang, Q. R. Zhao and Y. Xie, *Chem. Lett.*, 2004, **33**, 244.
15 J. X. Sun, G. Chen, J. Z. Wu, H. J. Dong and G. H. Xiong, *Appl. Catal. B-Environ.*, 2013, **132-133**, 304.
16 M. P. Brenner and D. Lohse, *Phys. Rev. Lett.*, 2008, **101**, 214505.
17 N. Tian, Z. Y. Zhou, S. G. Sun, Y. Ding and Z. L. Wang, *Science*, 2007, **316**, 732.
18 S. J. Guo, S. J. Dong and E. K. Wang, *ACS Nano*, 2010, **4**, 547.